Nonlinear Dyn (2007) 50:61–71
DOI 10.1007/s11071-006-9143-8

ORIGINAL ARTICLE

The effect of dynamical self-orientation and its applicability for identification of natural frequencies

Minvydas Ragulskis · Kazimieras Ragulskis

Received: 23 August 2005 / Accepted: 30 August 2006 / Published online: 5 January 2007

Abstract The effect of dynamical self-orientation and its applicability for the identification of natural frequencies of the investigated systems is demonstrated in this paper. Unidirectional vibration exciter is fixed to the investigated systems via a pivot link and can rotate around it. It is shown that the exciter changes its orientation in the steady state motion mode when the frequency of excitation sweeps over the fundamental frequency of the examined system. Approximate analytical analysis of the discrete system illustrates the basic principle of the effect of dynamical self-orientation. Numerical analysis of both the discrete and different continuous elastic systems confirms the applicability of the effect of self-orientation for the identification of natural frequencies.

Keywords Self-orientation · Natural frequencies · Pendulum · Vibration · Chaos

1 Introduction

Nonlinear pendulum is a paradigm in the study of oscillations and other phenomena in physics and nonlinear dynamics [1]. It has deserved much attention, from many viewpoints, including different model complexity, forcing, and damping aspects.

Pendulums are used in many different engineering applications, for many different purposes. Whenever a nonlinear pendulum is attached to an engineering structure, the dynamics of the whole system becomes rather complicated [2]. Computational analysis of such coupled systems comprising continuous and discrete elements is especially demanding [3, 4].

Typical applications where pendulums are attached to engineering structures include dynamic quenching of structural oscillations [5, 6]. Another, different but typical example is the excitation of engineering structures when a driven pendulum with a constant or periodic torque is attached to a continuous system [7, 8].

Vibration exciters can be represented as unidirectional shakers with an inertia mass oscillating along a straight guide. What would happen if such a vibration exciter would be attached to an elastic system via a pivot link and could rotate around it? This paper is focused on the excitation of structures by such generalized pendulums and nonlinear dynamical effects taking place in such systems.

2 Basic model of the system

The effect of dynamical self-orientation is demonstrated for a simple basic model presented in Fig. 1. All system components can perform only in-plane motions. Solid body 1 can move only along the y-axis in

M. Ragulskis (✉)
Department of Mathematical Research in Systems, Kaunas University of Technology, Studentu 50-222, Kaunas LT-51368, Lithuania
e-mail: minvydas.ragulskis@ktu.lt

K. Ragulskis
Department of Technical Sciences, Lithuanian Academy of Sciences, Vilnius, Lithuania

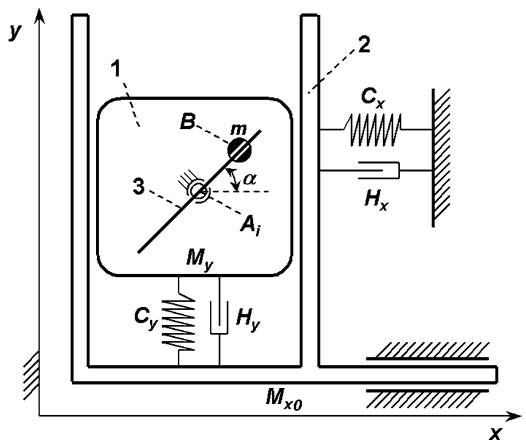

Fig. 1 Model of the basic system

its guide 2. In its turn, the guide 2 can move only along the x-axis. Mass of the body 1 is M_y; mass of the guide 2 is M_{x0}; bodies 1 and 2 are suspended on linear elastic springs and linear viscous dampers with appropriate coefficients: C_x, H_x, C_y, H_y. If no vibration exciters would be attached to body 1, there would exist two natural eigenfrequencies – one representing oscillations along the x-axis; another – along the y-axis. Such a basic model will help to demonstrate the principle of dynamical self-orientation when the vibration exciter aligns itself in the direction of the x-axis or the y-axis and this orientation is dependent on the frequency of excitation.

A unidirectional vibration exciter is fixed to the body 1 at point $A_i\,(x_i; y_i)$ via a pivot link and can rotate around it. The vibration exciter consists of two elements – a guide 3 and a mass m, which can move along the guide 3. The mass center of the guide 3 is located at the point A_i; its mass is incorporated into M_y. Inertia moment of the guide 3 is J. The movable mass m is located at point $B(x_B; y_B)$. The distance $z = |A_i B|$ is defined explicitly as a function of time (kinematic vibration excitation). The angle between guide 3 and the x-axis is α.

It is clear that

$$\begin{aligned} x_B &= x_i + z\,\cos\,\alpha; \\ y_B &= y_i + z\,\sin\,\alpha. \end{aligned} \tag{1}$$

Then the kinetic, potential, and dissipation energies of the system take the following form:

$$\begin{aligned} T &= 0,5\big(M_x\dot{x}_i^2 + M_y\dot{y}_i^2 + J\dot{\alpha}^2 + m\big(\dot{x}_i^2 + \dot{y}_i^2 + \dot{z}^2 \\ &\quad + z^2\dot{\alpha}^2 + 2\dot{x}_i(\dot{z}\,\cos\,\alpha - z\dot{\alpha}\,\sin\,\alpha) \\ &\quad + 2\dot{y}_i(\dot{z}\,\sin\,\alpha + z\dot{\alpha}\,\cos\,\alpha)\big)\big); \\ \Pi &= 0,5\big(C_x x_i^2 + C_y y_i^2\big); \\ D &= 0,5\big(H_x\dot{x}_i^2 + H_y\dot{y}_i^2 + H_\alpha\dot{\alpha}^2\big), \end{aligned} \tag{2}$$

where top dots denote full derivatives by time; $M_x = M_{x0} + M_y + m_0$; H_α is the coefficient of angular viscous damping of the pendulum.

It is assumed that the motion of the mass m is harmonic:

$$z = Z\cos(\omega t + \varphi), \tag{3}$$

where Z is the amplitude of oscillation; ω – angular velocity; φ – phase shift. Such a holonomic constraint reduces the four degree of freedom system (x_i; y_i; α and z) to a three degree of freedom system. Extended Lagrange equation results in the following system of second-order nonlinear ordinary differential equations:

$$\begin{aligned} &\ddot{x}_i + h_x\dot{x}_i + p_x^2 x_i = X_i; \\ &\ddot{y}_i + h_y\dot{y}_i + p_y^2 y_i = Y_i; \\ &J\ddot{\alpha} + H_\alpha\dot{\alpha} = L, \end{aligned} \tag{4}$$

where

$$\begin{aligned} X_i &= -\mu_x((\ddot{z} - z\dot{\alpha}^2)\cos\,\alpha - (z\ddot{\alpha} + 2\dot{z}\dot{\alpha})\sin\,\alpha); \\ Y_i &= -\mu_y((\ddot{z} - z\dot{\alpha}^2)\sin\,\alpha + (z\ddot{\alpha} + 2\dot{z}\dot{\alpha})\cos\,\alpha); \\ L &= -mz(z\ddot{\alpha} + 2\dot{z}\dot{\alpha} - \ddot{x}_i\sin\,\alpha + \ddot{y}_i\cos\,\alpha); \end{aligned} \tag{5}$$

$$h_x = \frac{H_x}{M_x + m}; \quad h_y = \frac{H_y}{M_y + m}; \quad p_x = \sqrt{\frac{C_x}{M_x + m}};$$

$$p_y = \sqrt{\frac{C_y}{M_y + m}}; \quad \mu_x = \frac{m}{M_x + m}; \quad \mu_y = \frac{m}{M_y + m}.$$

3 Approximate analysis of the basic model

It is clear that full investigation of the basic model requires solution of the set of nonlinear differential equations in Equation (4). Nevertheless, analytical approximation can be straightforward under the assumption that the angle α is almost stationary in a steady state regime of motion. In that case, the term L must be small:

$$J\ddot{\alpha} + H_\alpha\dot{\alpha} = \varepsilon L, \tag{6}$$

where ε is a small positive constant. Then the system variables are expanded in power series of ε:

$$\begin{aligned} &\alpha = \alpha_0 + \varepsilon\alpha_1 + \cdots; \\ &x_i = x_{i0} + \varepsilon x_{i1} + \cdots; \\ &y_i = y_{i0} + \varepsilon y_{i1} + \cdots. \end{aligned} \tag{7}$$

Collecting the terms at the zeroth order of ε produces:

$$\begin{aligned} &\alpha_0 = \text{const}; \\ &x_{i0} = \frac{\mu_x Z\omega^2 \cos\alpha_0}{D_x}\left(\left(p_x^2 - \omega^2\right)\cos\omega t + h_x\omega\sin\omega t\right); \\ &y_{i0} = \frac{\mu_y Z\omega^2 \sin\alpha_0}{D_y}\left(\left(p_y^2 - \omega^2\right)\cos\omega t + h_y\omega\sin\omega t\right). \end{aligned} \tag{8}$$

where

$$\begin{aligned} &D_x = \left(p_x^2 - \omega^2\right)^2 + (h_x\omega)^2; \\ &D_y = \left(p_y^2 - \omega^2\right)^2 + (h_y\omega)^2. \end{aligned} \tag{9}$$

Next, small motion around α_0 can be found from the equation

$$J\ddot{a}_1 H_a \dot{a}_1 = L_0, \tag{10}$$

where L_0 is the approximation of L at $a = a_0$; $x_i = x_{i0}$; $y_i = y_{i0}$:

$$L_0 = -mZ(-\ddot{x}_{i0}\,\sin a_0 + \ddot{y}_{i0}\,\cos a_0). \tag{11}$$

The removal of the secular terms from Equation (11) leads to the condition:

$$\bar{L}_0 = \frac{mZ^2\omega^4}{4} D\,\sin(2a_0) = 0, \tag{12}$$

where the top line denotes averaging by time, and

$$D = -\mu_x\frac{p_x^2 - \omega^2}{D_x} + \mu_y\frac{p_y^2 - \omega^2}{D_y}. \tag{13}$$

Equation (12) produces two solutions:

$$\begin{aligned} &(\alpha_0)_1 = \pi n; \\ &(\alpha_0)_2 = \frac{\pi}{2} + \pi n. \end{aligned} \tag{14}$$

The stability condition is determined from Equations (10) and (15):

$$-D\,\cos(2\alpha_0) > 0. \tag{15}$$

Thus, $(\alpha_0)_1$ is stable and $(\alpha_0)_2$ is unstable when $D < 0$, and vice versa when $D > 0$. The critical frequencies at which the stability of solutions, represented by Equation (14), change can be determined from the following equation, which is a third-order polynomial in terms of ω^2:

$$\begin{aligned} &\left(-\mu_x\left(p_y^2 - \omega^2\right) + \mu_y\left(p_x^2 - \omega^2\right)\right)\left(p_x^2 - \omega^2\right)\left(p_y^2 - \omega^2\right) \\ &\quad + \left(-\mu_x\left(p_x^2 - \omega^2\right)h_y^2 + \mu_y\left(p_y^2 - \omega^2\right)h_x^2\right)\omega^2 = 0. \end{aligned} \tag{16}$$

When the linear damping coefficients are small, the solution of Equation (16) can be approximated as follows:

$$\omega^2 = \omega_0^2 + \varepsilon\omega_1^2 + \cdots \tag{17}$$

on the assumption that h_x and h_y are small:

$$\begin{aligned} &h_x = \varepsilon h_x; \\ &h_y = \varepsilon h_y. \end{aligned} \tag{18}$$

Solving Equation (16) up to linear terms of ε produces three approximate roots:

$$\begin{aligned} &(\omega^2)_1 \cong p_x^2 + h_x^2\frac{\mu_y}{\mu_x}\frac{p_x^2}{p_x^2 - p_y^2}; \\ &(\omega^2)_2 \cong p_y^2 + h_y^2\frac{\mu_x}{\mu_y}\frac{p_y^2}{p_y^2 - p_x^2}; \\ &(\omega^2)_3 \cong \frac{-\mu_y p_x^2 + \mu_x p_y^2}{\mu_x - \mu_y} \\ &\qquad + \left(h_y^2\frac{\mu_x}{\mu_y} + h_x^2\frac{\mu_y}{\mu_x}\right)\frac{-\mu_y p_x^2 + \mu_x p_y^2}{(\mu_x - \mu_y)\left(p_x^2 - p_y^2\right)}. \end{aligned} \tag{19}$$

It can be noted that the third root will exist only if $(\omega^2)_3 > 0$. If the third root does not exist, and

$$p_x^2 < p_y^2 \tag{20}$$

the vibration exciter will oscillate in the direction of x-axis at following frequencies:

$$0 < \omega < \omega_1 \quad \text{or} \quad \omega_2 < \omega < \infty. \tag{21}$$

If

$$\omega_1 < \omega < \omega_2 \tag{22}$$

then the vibration exciter will oscillate in the direction of y-axis. Also, in that case, $(\omega^2)_1$ is slightly lower than p_x^2 and $(\omega^2)_2$ is slightly higher than p_y^2.

These approximate analytical results lead to an important conclusion. A unidirectional vibration exciter with an additional angular degree of freedom can be used for the identification of natural frequencies of elastic structures. The vibration exciter should settle to either vertical or horizontal direction in the steady state motion mode depending on the frequency of excitation. The first critical frequency separating vertical and horizontal motions will be an estimate of the fundamental frequency of the structure.

4 Numerical analysis of the basic system

The set of differential equations of motion in Equation (3) is solved using direct time marching techniques. The results of simulation are presented in the Poincare diagram in Fig. 2. At every discrete value of ω, time marching is continued until the transient processes cease down. Then, the trajectories in phase plane $\alpha - \dot{\alpha}$ are sectioned by plane $\dot{\alpha} = 0$. It can be noted that the vibration exciter can rotate in a steady state regime of motion and thus plotting of α could be quite complicated due to possible boundlessness of α. Therefore, every value of α produced by Poincare sectioning is mapped into the interval $[-\pi, \pi]$ by simple modulus 2π transformation adding or subtracting $2\pi k$ with appropriate $k \in \mathbf{Z}$.

The amplitude of oscillation Z is decreased at increasing ω to preserve constant maximum kinetic energy of the exciter (at constant α):

$$(T_{\mathrm{V}})_{\max} = \frac{m\,((\dot{z})_{\max})^2}{2} = \frac{m\,(Z\omega)^2}{2} = \text{const}, \tag{23}$$

where T_{V} – kinetic energy of the vibration exciter. The following parameters were selected for numerical simulation: $m = 0.1$; $M_x = 2$; $M_y = 1$; $C_x = 1$; $C_y = 1$; $h_x = 0.05$; $h_y = 0.05$. The following parameters are calculated using Equations (4) and (19):

$$p_x \approx 0.690; \quad p_y \approx 0.954; \quad \omega_1 \approx 0.686; \quad \omega_2 \approx 0.976. \tag{24}$$

Figure 2 shows excellent correlation between analytical and numerical analysis. In the region $0 < \omega < \omega_1$, the exciter is oscillating in the x-axis direction (angle α is zero in the steady state regime of motion). The transient process is illustrated in Fig. 3 at $\omega = 0.4$.

The exciter orients itself in the direction of y-axis (angle α equal to $\pi/2$ or $-\pi/2$) in the frequency range $\omega_1 < \omega < \omega_2$. The transient dynamics is illustrated in Fig. 4 at $\omega = 0.7$. Chaotic system response is observed in a relatively short frequency range around $\omega = 0.75$.

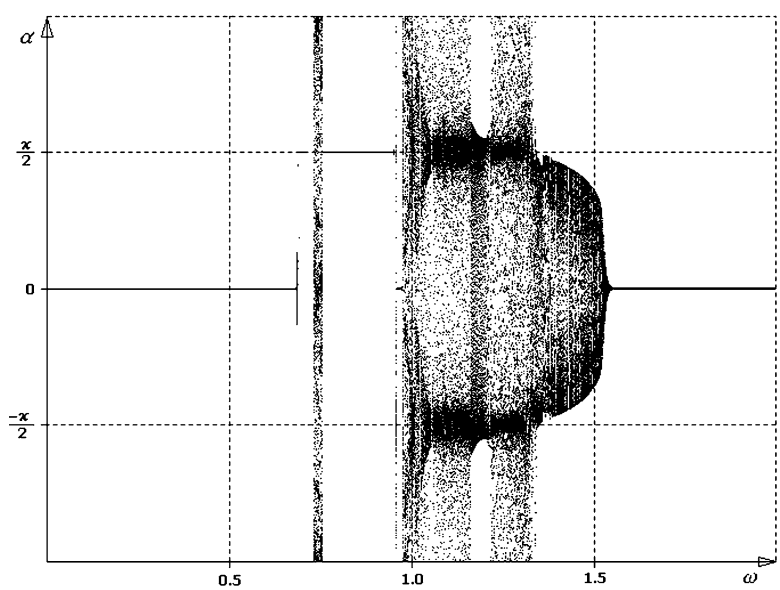

Fig. 2 Poincare map at $m = 0.1$; $M_x = 2$; $M_y = 1$; $C_x = 1$; $C_y = 1$; $H_\alpha = 0.05$; $h_x = 0.05$; $h_y = 0.05$; $Z = \frac{0.15}{\omega}$

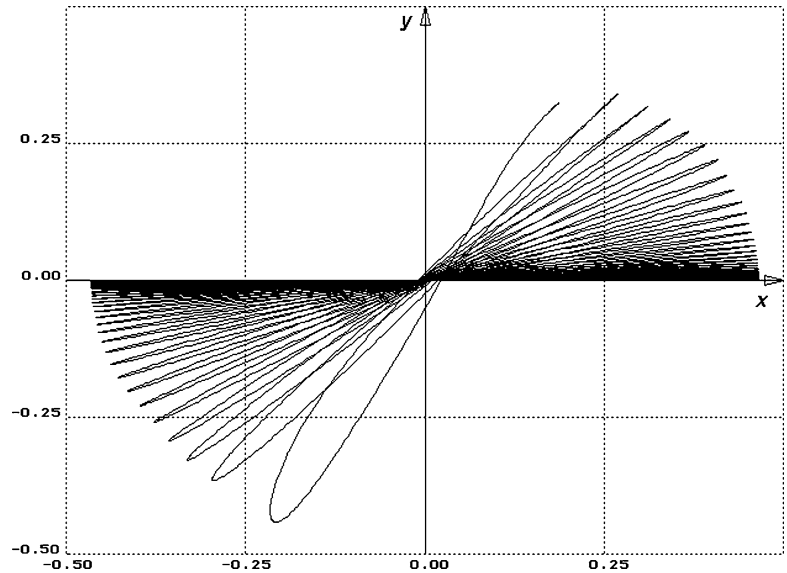

Fig. 3 Transient dynamics at $\omega = 0.4$

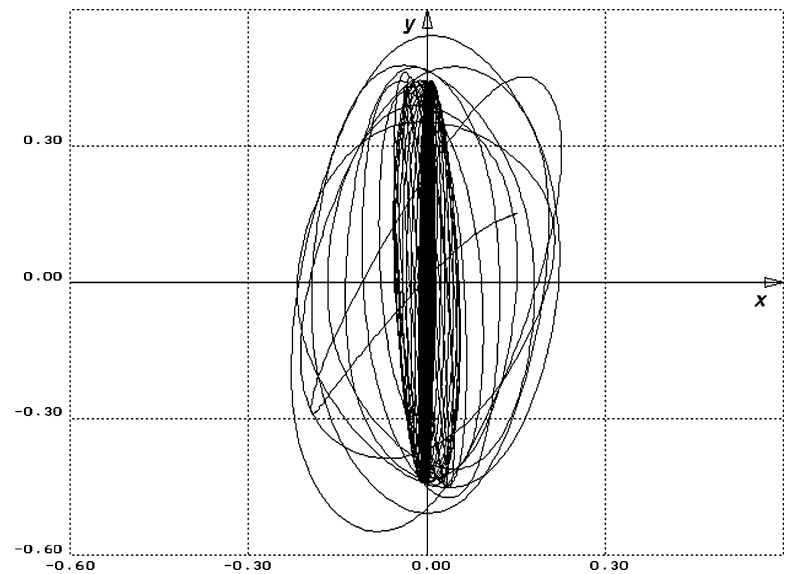

Fig. 4 Transient dynamics at $\omega = 0.7$

Finally, the vibration exciter again orients itself in the direction of x-axis in the frequency range $\omega_2 < \omega < \infty$. It can be noted that a burst of chaotic motion is observed in the region just over ω_2. This chaotic motion is illustrated in Figs. 5 and 6. The exciter tries to settle around $\alpha = \pi/2 + \pi k$, $k \in \boldsymbol{Z}$, but these solutions are already unstable in this frequency range. Time moments when the pendulum crosses the vicinity of $\alpha = \pi/2 + \pi k$ are marked by circles in Fig. 6. Such a diagram provides insight into the complexity of the chaotic response where both the direction of the jump and the duration of the stay around the unstable solutions are random.

Finally, it can be noted that the regions of chaotic response shrink at lower values of the exciter's mass m and the amplitude Z. But, in that case, the time lengths of the transient processes are extended, which is quite a natural result.

5 Computational issues for an elastic structure coupled with a discrete self-orientating exciter

Numerical models of elastic continuous systems are built exploiting finite-element techniques [9]. Meshing of a continuous structure produces matrix ordinary

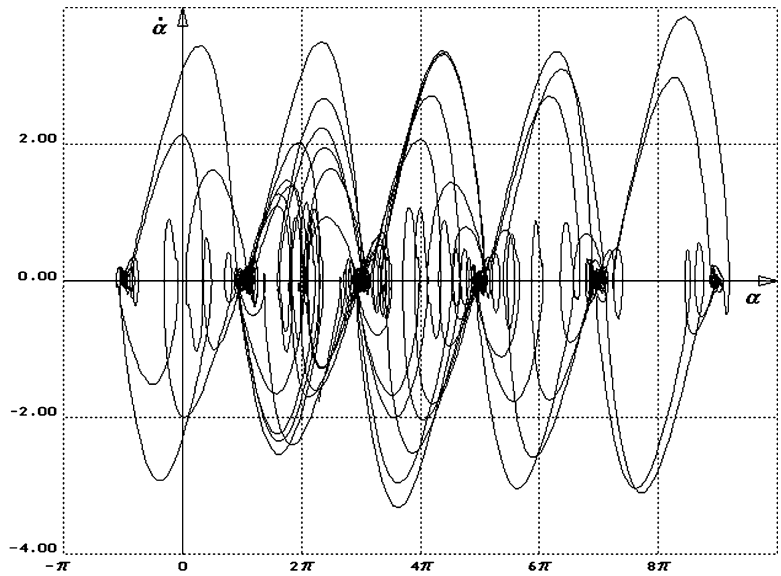

Fig. 5 Transient dynamics at $\omega = 1.1$

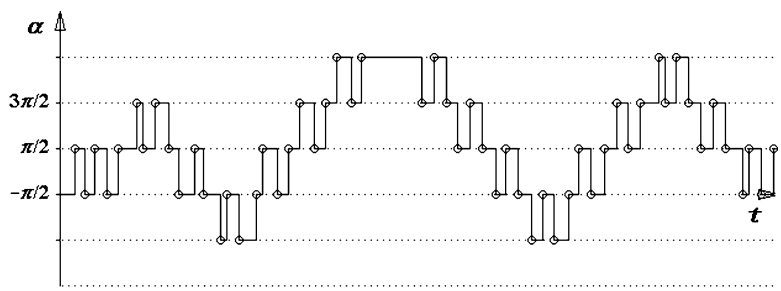

Fig. 6 Transient dynamics at $\omega = 1.1$

differential equation of the following form:

$$[M]\{\ddot{X}\} + [H]\{\dot{X}\} + [C]\{X\} = \{F\}, \tag{25}$$

where $[M]$, $[H]$, $[C]$ – represent mass, damping, and stiffness matrixes appropriately; $\{\ddot{X}\}$, $\{\dot{X}\}$, $\{X\}$ – represent global vectors of acceleration, velocity, and displacement; $\{F\}$ – represents the vector of external forces. Every node (except boundary nodes) corresponds to two degrees of freedom (two ordinary differential equations) for models describing in-plane motions; one – to motions in the direction of the x-axis, another – in the direction of the y-axis.

Self-orientating exciter is represented by three second-order ordinary differential equations – two corresponding to in-plane motions; one – rotation (Eqs. (4) and (5)). The exciter can be attached to any point of the elastic structure, but it is natural to assume that it is attached to one of the nodes of the continuous system meshed by finite-element techniques. Let us denote two degrees of freedom corresponding to the node to which the exciter is attached as r (corresponding to displacement in the direction of the x-axis) and s (corresponding to displacement in the direction of the y-axis).

Then, the nonlinear dynamical effects caused by the self-orienting vibrator are evaluated through the external force terms on the right sides of the rth and sth differential equations in the matrix system of equations, represented by Equation (25). Also, an additional differential equation corresponding to the rotation of the exciter around the pivot node must be added that increases the number of degrees of freedom by one. The right sides of the rth and sth differential equations take the following form (see Equations (4) and (5)):

$$\begin{aligned} f_r &= -m(\ddot{x}_r + (\ddot{z} - z\dot{\alpha}^2)\cos\alpha - (z\ddot{\alpha} + 2\dot{z}\dot{\alpha})\sin\alpha); \\ f_s &= -m(\ddot{x}_s + (\ddot{z} - z\dot{\alpha}^2)\sin\alpha + (z\ddot{\alpha} + 2\dot{z}\dot{\alpha})\cos\alpha), \end{aligned} \tag{26}$$

where f_r and f_s are rth and sth components of vector $\{F\}$ in Equation (25). A separate differential equation describing the variation of angle α (rotation) takes the following form (see Equation (5)):

$$J\ddot{\alpha} + H_\alpha\dot{\alpha} = -mz(z\ddot{\alpha} + 2\dot{z}\dot{\alpha} - \ddot{x}_r \sin\alpha + \ddot{x}_s \cos\alpha) \tag{27}$$

Analysis of a continuous structure coupled with a discrete system is a computationally demanding problem, especially when one of the systems is linear and another – nonlinear [3]. The terms $m\ddot{x}_r$ and $m\ddot{x}_s$ in Equation (26) are brought from the right side to the left side of corresponding differential equations in order to preserve the stability of numerical time marching codes. Thus, the mass matrix of the elastic structure in Equation (25) is augmented. The mass m is added to the diagonal elements in the rth and sth lines of the mass matrix (note the minus signs at terms $m\ddot{x}_r$ and $m\ddot{x}_s$ in Equation (26)). This augmentation naturally represents the mass increase of the node to which the vibration exciter is attached.

Analogous to the basic model, it is assumed that z is a predefined harmonic process (Equation (3)). Then the governing differential equations (Equations (25–27)) can be solved simultaneously using direct time marching techniques.

6 Identification of fundamental frequency of an elastic cantilevered plate

Initially, eigenshapes and natural frequencies of an elastic structure are calculated (with the augmented mass matrix; $m = 0.1$). The first four eigenshapes of a cantilevered plate are presented in Fig. 7 where grey lines stand for the structure in the status of equilibrium; dark solid lines – for appropriate in-plane eigenshapes; black dots represent the node to which the self-orientating exciter is attached. Natural frequencies are printed at the bottom of appropriate eigenshapes.

Next, the transient processes are analyzed at different frequencies of excitation. In our model, $r = 23$ (the degree of freedom representing the motion of the node to which the exciter is attached in the direction of the x-axis) and $s = 24$ (same node in the direction of the y-axis). Transient process at $\omega = 0.4$ is presented in Fig. 8; at $\omega = 0.65$ – in Fig. 9. It can be clearly seen that at $\omega = 0.4$, the angle α settles at 0, while the node to which the exciter is attached oscillates in the direction of the x-axis (the same direction as the exciter itself). On the contrary, at $\omega = 0.65$, the angle α settles at $\pi/2$, while both the node and the exciter oscillate in the direction of the y-axis. That is even more clearly illustrated in the phase plane x–y in Fig. 10 where the transient dynamics of all nodes of the structure is plotted simultaneously.

Finally, the Poincare map is constructed for steady state processes at different frequencies of excitation (Fig. 11). It can be seen that the regime of motion at $\alpha = 0$ loses its stability at frequencies around 0.5. Then, the process stabilizes again around $\omega = 0.6$, but already around $\alpha = (\pi/2)$. That gives an estimate that the first fundamental frequency of the system under investigation is in the region $0.5 < \omega < 0.6$, which is a rather good estimate (Fig. 7).

Such an estimate can be explained by the following considerations. If a system is excited at a frequency lower than its fundamental frequency (unidirectional harmonic excitation in any possible direction), then the amplitude of the structure's response (in the steady state motion mode) will be highest in the direction corresponding to motion according to its fundamental eigenshape. The effect of self-synchronization between the excited structure and the exciter takes place. The exciter orients itself in such a direction, which can generate maximum amplitude of the excited system.

When the frequency of excitation approaches the second natural frequency, the direction of the maximum

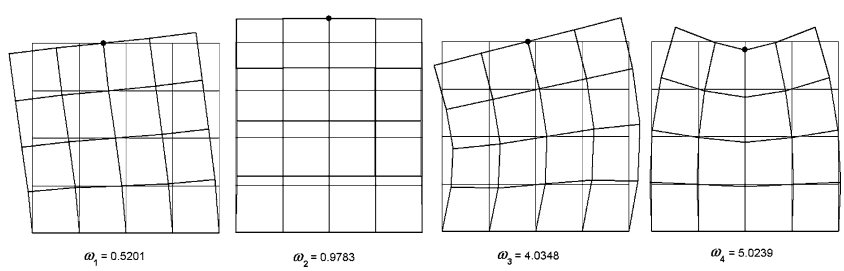

Fig. 7 The first four eigenshapes and natural frequencies of the elastic structure

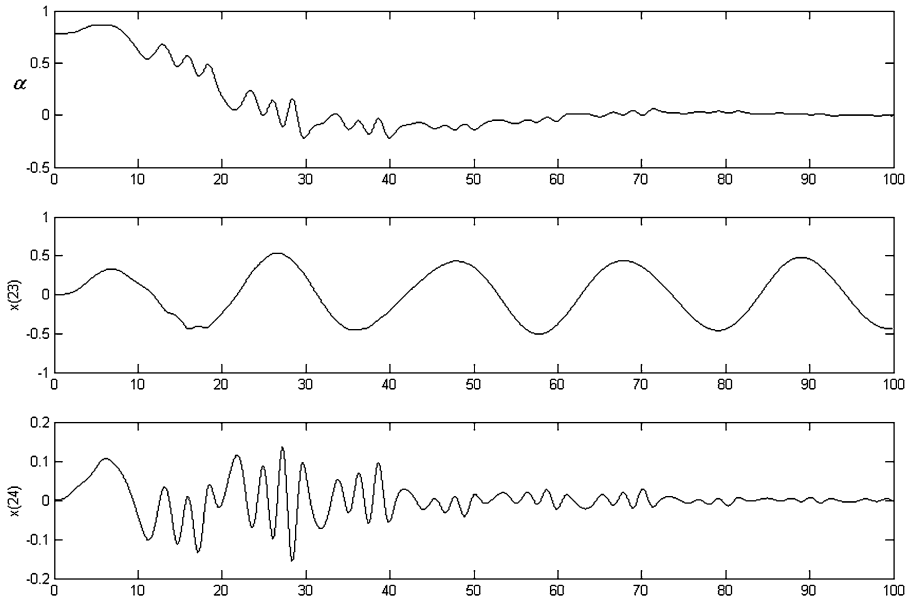

Fig. 8 α, x_r and x_s versus time – transient process at $\omega = 0.4$

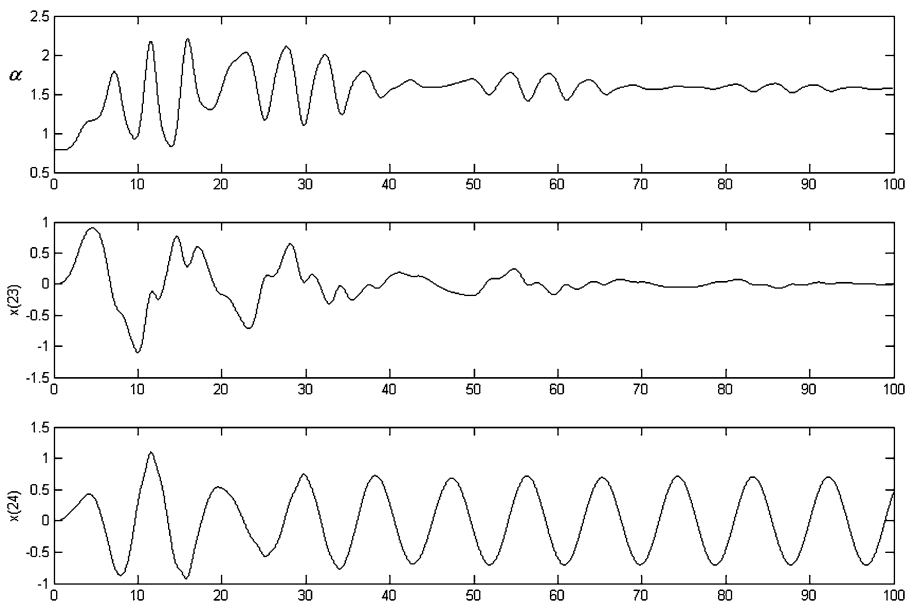

Fig. 9 α, x_r and x_s versus time – transient process at $\omega = 0.65$

amplitude of the structure's response already coincides with the direction corresponding to motion according to its second eigenshape. Again, the effect of self-synchronization orients the exciter to the direction according to the second eigenshape of the structure.

Better estimates of the fundamental frequency can be achieved if either the mass m or the amplitude Z is decreased. But then, as mentioned previously, the length of the transient processes becomes large.

Different nodes could be selected for attachment of the vibration exciter. General recommendation would be to select such nodes, which are most sensitive to external excitation. In our example, it would not be a good idea to select a node near the fastened bottom nodes. In principle, the observed phenomena would be

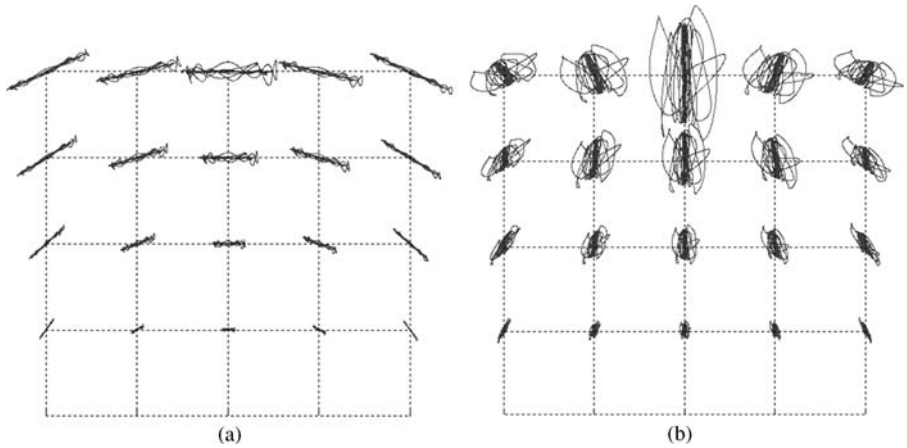

Fig. 10 Transient processes (traces of the nodes) in the phase plane at $\omega = 0.4$ (a) and $\omega = 0.65$ (b); *dashed mesh* represents the structure in the state of equilibrium

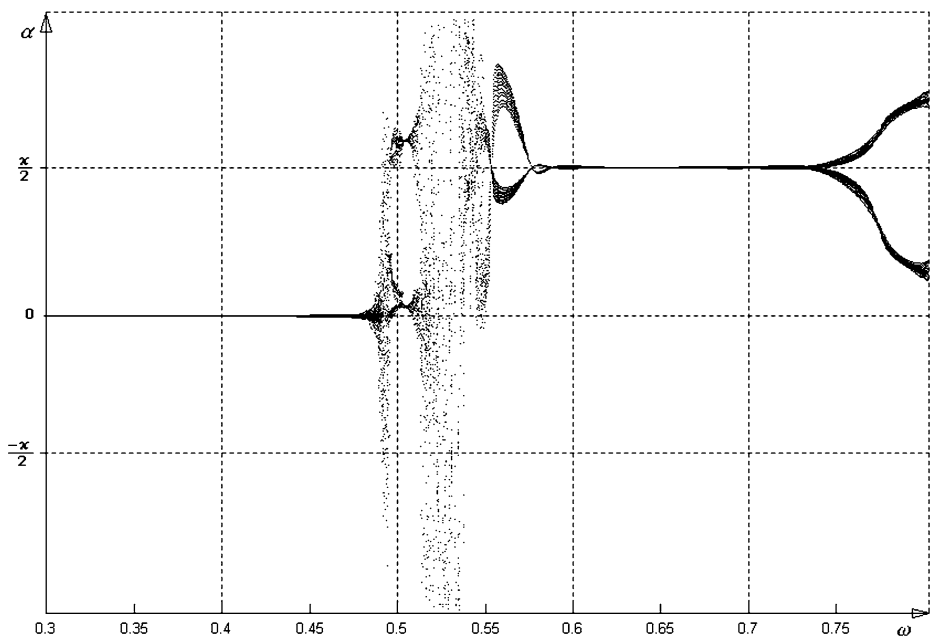

Fig. 11 Poincare map of the node to which the exciter is attached

the same, but the sensitivity and the accuracy of the estimates would be considerably decreased.

7 Identification of fundamental frequency of elastic ring with internal clamped radius

A much more complex system is analyzed in this section. The first eight eigenshapes of an elastic ring with internal clamped radius are presented in Fig. 12 with appropriate eigenfrequencies printed inside every drawing of eigenshape. Finite-element mesh in the state of equilibrium is shown in grey lines; deformed mesh according to eigenshpe – in black lines. Black dot shows the node to which the vibration exciter is attached.

It can be seen that at least the first eigenshapes of the described system can be classified according to the type of the dominant oscillation – angular or radial oscillation. The nodes of the structure perform angular oscillations when the ring vibrates according to its first

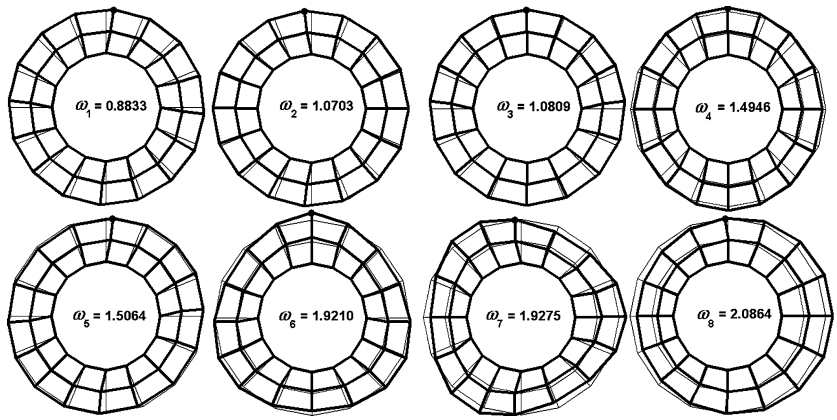

Fig. 12 First eigenshapes of an elastic ring with internal clamped radius

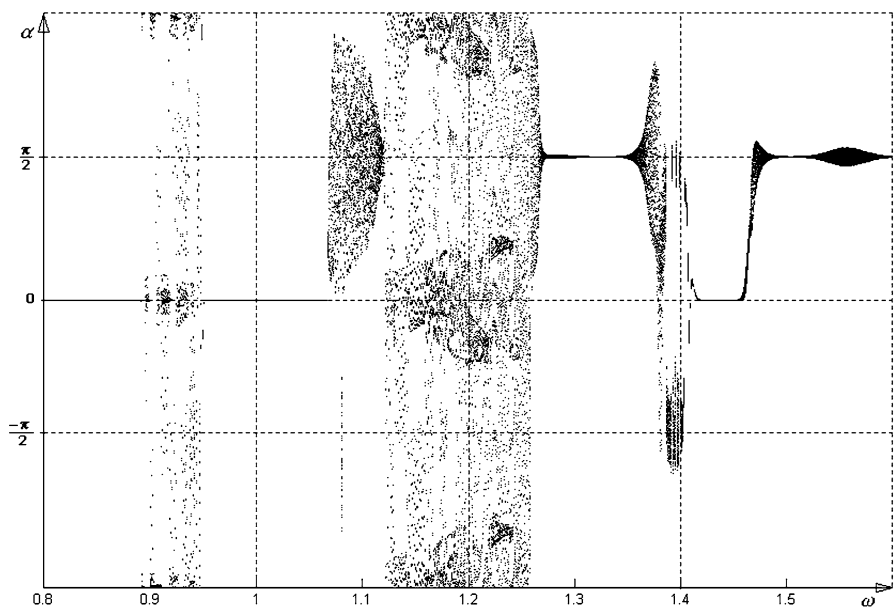

Fig. 13 Poincare map of the node to which the exciter is attached

eigenshape. The second and the third eigenshapes are also angular eigenshapes. By the way, the second and the third eigenshapes would be coupled eigenshapes (same frequency) if the vibration exciter would not be attached and the mass matrix of the system would not be augmented. The fourth eigenshape is already a radial eigenshape.

As demonstrated in the previous examples, the self-orientating vibration exciter can classify different eigenshapes. The major difference now is that the first three eigenshapes of the elastic ring are of the same type. So, it is hard to expect that the self-orientating vibration exciter could distinguish the first eigenshape from the second one. But the fourth eigenshape is already different from the first three ones – the nodes now oscillate also in the radial direction. Therefore, one can expect that the self-orientating exciter will exhibit tendency to orient itself in the radial direction at the frequencies over ω_3. Really, the Poincare map (Fig. 13) of the node to which the self-orientating vibration exciter is attached demonstrates that the stability of the vibrator's motion in the angular direction is lost over the frequency equal to 1.08. This is a very good result demonstrating that the effect of self-orientation can be applied also for rather complex elastic structures.

Finally, it can be noted that the oscillating mass and the amplitude of oscillations of the exciter must be relatively low compared to the structure under investigation in order to provide sufficiently accurate estimates.

8 Concluding remarks

The effect of self-orientation is presented and illustrated in this paper. A vibration exciter with an additional angular degree of freedom can serve as a detector of natural frequencies. Approximate analytical analysis of a basic model provides insight into the principles of dynamical self-orientation. It is shown that the self-orientating vibration exciter can discriminate different eigenshapes of elastic structures to which it is attached. This effect can be applicable for the detection of fundamental frequencies of different elastic structures.

It can be noted that only in-plane vibrations are considered in this paper. Three-dimensional systems, vibration exciters with limited power, experimental analysis of the effect of self-orientation – all these are definite objects of future research.

References

1. Trueba, J.L., Baltanás J.P., Sanjuán, M.A.F.: A generalized perturbed pendulum. Chaos Solitons Fractals **15**(5), 911–924 (2003)
2. Omar, H.M., Nayfeh, A.H.: Anti-swing control of gantry and tower cranes using fuzzy and time-delayed feedback with friction compensation. Shock Vib. **12**(2), 73–90 (2005)
3. Belato, D., Weber, H.I., Balthazar, J.M.: Using transient and steady state considerations to investigate the mechanism of loss of stability of a dynamical system. Appl. Math. Comput. **164**(2), 605–613 (2005)
4. Tsai, C.S., Chiang, T.C., Chen, B.J.: Finite element formulations and theoretical study for variable curvature friction pendulum system. Eng. Struct. **25**(14), 1719–1730 (2003)
5. Vyas, A., Bajaj, A.K.: Dynamics of autoparametric vibration absorbers using multiple pendulums. J. Sound Vib. **246**(1), 115–135 (2001)
6. Murnal, P., Sinha, R.: A seismic design of structure–equipment systems using variable frequency pendulum isolator. Nucl. Eng. Des. **231**(2), 129–139 (2004)
7. Song, Y., Sato, H., Iwata, Y., Komatsuzaki, T.: The response of a dynamic vibration absorber system with a parametrically excited pendulum. J. Sound Vib. **259**(4), 747–759 (2003)
8. Belato, D., Weber, H.I., Balthazar, J.M., Mook, D.T.: Chaotic vibrations of a nonideal electro-mechanical system. Int. J. Solids Struct. **38**(10–13), 1699–1706 (2001)
9. Bathe, K.J.: Finite Element Procedures in Engineering Analysis. Prentice-Hall, Englewood Cliffs, NJ (1982)